Smart Antennas Based on Spatial Multiplexing of Local Elements (SMILE) for Mutual Coupling Reduction

Jonathan D. Fredrick, *Member, IEEE*, Yuanxun Wang, *Member, IEEE*, and Tatsuo Itoh, *Fellow, IEEE*

***Abstract*—A new method for reducing mutual coupling in a smart antenna array using patch antenna elements is proposed. In a recently introduced smart antenna architecture, the spatial multiplexing of local elements (SMILE) scheme, the newly proposed array feed network affects mutual coupling. It is demonstrated that proper design of the feed network may reduce mutual coupling significantly, yielding nearly ideal radiation characteristics. Numerical solutions are used to study and optimize the currents on the surface of a four-element C-band patch antenna array and feed network. Radiation patterns of the same array with different feed networks are also computed. Results show a reduction in sidelobe level of several decibels, increased accuracy in beam pointing during scan, and improved null depth and placement.**

***Index Terms*—Digital beamforming, feed network, mutual coupling, patch antenna, smart antenna, spatial multiplexing, spatial multiplexing of local elements (SMILE).**

I. Introduction

SMART antennas evolving from traditional phased arrays have found numerous applications in modern wireless communications. The adaptive beamforming capability in smart antenna systems enables flexible synthesis and steering of antenna beams for optimized signal-to- noise and interference ratio performance. Conventional smart antennas are based on the process of vector channel information from each antenna element; therefore the number of radio-frequency (RF) channels, such as low-noise amplifiers and mixers, has to equal the number of antenna elements, which often results in great hardware expense. A new type of smart antenna based on the spatial multiplexing of local elements (SMILE) approach has recently been introduced [1]. This new type of smart antenna reduces hardware requirements to a single RF channel while retaining all of the signal's vector information. Thus advanced signal-processing algorithms for digital beamforming and direction of arrival (DOA) estimation may be performed. The essential idea of the SMILE approach is to sample the incoming signal envelope above the Nyquist rate in the antenna so that all the information is carried in the format of pulsed signal chains. Those signal chains are then multiplexed to form a single-channel RF output to the RF front-end. After downconversion to the intermediate frequency (IF) or baseband, the signal can be demultiplexed and filtered in the post stages to restore the original signal information arriving at each antenna element.

From an antenna design perspective, a few benefits are associated with this novel design besides the front-end hardware expense reduction. First, the feed-line outputs are reduced to one, which saves space in antenna array layout and simplifies the interconnection between the antennas and front-end hardware. Second, since only one antenna is turned on at one time during the sampling process, the mutual coupling effect between different antenna elements may be reduced assuming the feed-line network is designed properly. The objective of this paper is to study how the mutual coupling of the SMILE array is affected by the feed-line network. More importantly, a proper way of designing the feed lines is proposed to reduce the mutual coupling in this novel smart antenna array.

It is well known that mutual coupling negatively affects pattern synthesis and DOA estimation accuracy; hence the reduction of said is of great interest [2]–[4]. Many efforts have been carried out in the past to address mutual coupling issues in antenna arrays. The often used mutual coupling modeling techniques include the Z-approach based on network theory [5], [6] and the active element pattern approach based on mean square fitting calibration [7]–[10]. Su and Ling have demonstrated that the Z-approach is limited for strongly resonating antennas while the active element pattern approach is generally valid based on the method of moments theory, except in the case when the coupling coefficient exhibit strong angular dependence [11]. For compensation of the mutual coupling error based on the active element pattern approach, a coupling matrix is usually measured and the inverse of matrix is then formulated to weight the incoming signals in order to cancel the coupling effect; this may incur great computational burden in the digital beamforming process.

In this paper, rather than proposing a new algorithm, it will be demonstrated that an appropriate design of the SMILE array can reduce the mutual coupling to a minimum. The essential idea is to minimize the parasitic current on antenna elements by changing the load impedance, which is determined by the length of the feed line when the element is turned OFF. Thus the parasitic radiation field caused by the adjacent elements can be reduced so that the active element pattern approaches the single element pattern.

Manuscript received August 16, 2002; revised November 1, 2002.

J. D. Fredrick was with the Department of Electrical Engineering, University of California, Los Angeles, CA 90095 USA. He is now with Raytheon Space and Airborne Systems, El Segundo, CA 90245 USA (e-mail: jfredrick@ieee.org).

Y. Wang and T. Itoh are with the Department of Electrical Engineering, University of California, Los Angeles, CA 90095 USA.

Digital Object Identifier 10.1109/TAP.2003.818798

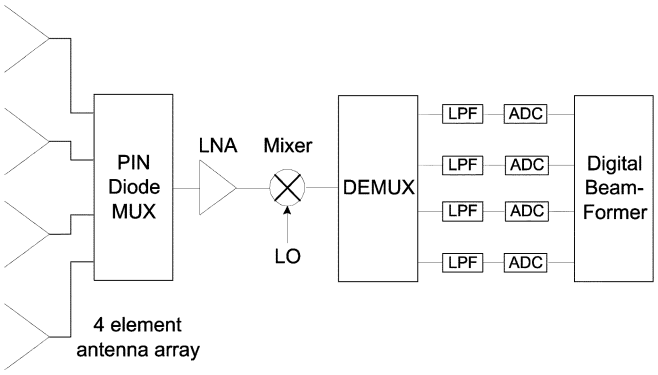

Fig. 1. SMILE system block diagram.

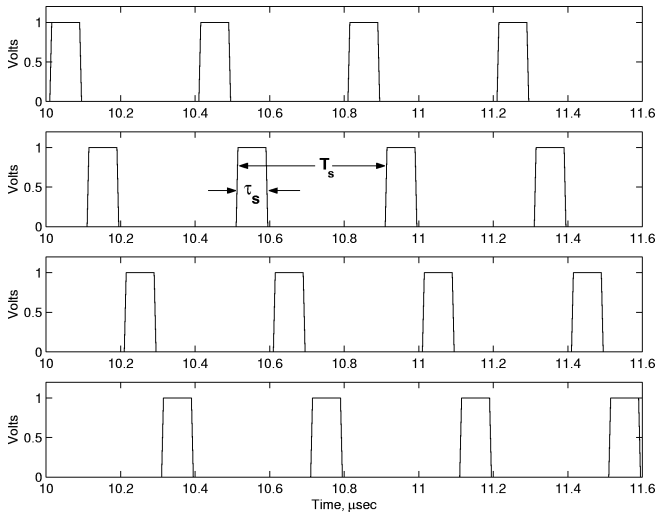

Fig. 2. Digital sequence switch timing diagram.

We shall investigate the effect that the switching device's location has upon mutual coupling on a four-element patch antenna array. Full-wave electromagnetic simulators such as finite-difference time-domain (FDTD) and method of moments (MoM) codes are implemented to obtain an understanding of how the location of the switching device in the feed network may be used to reduce surface currents on adjacent elements. By choosing an optimum location, ultimately the active element pattern can be improved to nearly the single-element pattern.

In this paper, the basic operating principles of the SMILE array are first described along with the system block diagram. Array performance in signal-to-noise ratio and diversity gain is briefly discussed. The antenna array feed network integrated with a PIN diode multiplexing circuit is illustrated as a key building block of the system and presents motivation for this paper. Then measured data are given to validate the system concept and the performance of the feed network. The effects of the array feed network upon mutual coupling are then investigated with FDTD and MoM. To show that mutual coupling may be reduced, surface current plots, active element patterns, and array radiation patterns are given to illustrate the effectiveness of the reduction techniques.

II. System Principles

The block diagram of the SMILE system proposed in [1] is shown in Fig. 1. The system consists of an antenna array with integrated multiplexing network, a digital sequence generator (not shown), a single RF channel including low-noise amplifier (LNA), mixer, analog demultiplexer, low-pass filters, analog-to-digital (A/D) sampling circuitry, and digital signal processor (DSP). The multiplexing network, made of an Agilent HPND-4005 PIN diode in series with the feed of each antenna element, is driven by the digital sequence generator so that the N channels of signal from N antenna elements are sequentially multiplexed to form a single-channel RF output. The switch-driving waveform is shown in Fig. 2, where $\tau_s = 0.1\ \mu$s. Considering a signal from one of the elements with carrier frequency f_c and modulation bandwidth B, the multiplexing acts as a sampling process with rectangular pulses of width τ_s and periodicity T_s. The spectrum of the multiplexed signal is spread by the sampling process, as determined by the Fourier transform of the sampling function. As a result, the bandwidth of cascaded system components needs to be adequate. Details of the effects of sampling on signal spectra are given in the literature [1]. The LNA used in this design is a connectorized unit from Miteq with 25-dB gain and a 2-dB noise figure. The system illustrated here applies to a receiver.

At this time, a transmitter utilizing this type of technology has not been developed. To transmit a large amount of power, it is desirable to have multiple amplifiers working in parallel. Additionally, if the transmit amplifiers or antennas are switched in time, the radiation pattern will not be that of the array but of the single ON element.

After the multiplexing, the single-channel RF output is amplified and downconverted to baseband or an IF depending upon mixer configuration. The analog demultiplexer, driven by the same sequence generator, is then used to separate the signal into different channels. To restore the original modulation information, a low-pass filter can be used to reconstruct the continuous signal from the samples. The cutoff frequency $f_{\rm lpf}$ of the filters is selected to allow the basic modulation frequency components to pass. In order to prevent aliasing, the low-pass filter cutoff is defined as

$$\frac{B}{2} < f_{\rm lpf} < f_s - \frac{B}{2}. \tag{1}$$

The signal is then digitized by the A/D converters. The beamforming is carried out in the digital domain. If the system is configured as a heterodyne downconverter, then a bandpass filter is needed and the final conversion to baseband may be done in the digital domain. The spectral efficiency of the modulation used must be considered when selecting the sampling rate and filter cutoff, since a spectrally inefficient modulation scheme, such as binary phase-shift keying (BPSK) without pulse shaping, will consume more bandwidth in practice than the data rate suggests.

A. Carrier-to-Interference (C/I) Performance and Combining Gain

One of the goals of the SMILE system is to achieve the same C/I performance as traditional phased and smart antenna arrays without the substantial hardware costs. In a noisy environment, the C/I is defined as a ratio of the incident carrier signal

power over the interference and environment noise before demodulation. Assuming a nonfading case, the combining gain is defined as the C/I improvements of the SMILE array over the single antenna case. To carry out a qualitative analysis, we consider the signal-of-interest (SOI) and noise, or signal-not-of-interest (SNOI), to impinge upon the antenna array. Since the antenna has a bandlimiting function, external white noise becomes bandlimited in the system and thus may be considered as a bandlimited SNOI. For purposes of analysis, it is assumed that the system is ideal and noiseless. It is also assumed that the antenna's bandwidth is matched to the signal bandwidth. The sampling process affects the spectrum of both the received SOI and SNOI. When the envelopes of the SOI and SNOI are sampled, their spectrums both spread according to the Fourier transform of the sampling function. The SOI and SNOI are then downconverted and passed through the low-pass filters. At this point the in-band C/I has remained constant; however, the in-band signal energy for both SOI and SNOI has been reduced by a factor of N^2 compared to those of the conventional array. When the beamforming algorithm is applied, the SOI samples add coherently and the SNOI does not. This provides a factor of N increase in C/I. Thus the combining gain of SMILE array is N, the same as that of conventional smart antennas. In order to achieve the maximum combining gain, it is crucial to design the antenna bandwidth to match the system bandwidth. If the antenna has a broader bandwidth than the SOI and greater than the system sampling speed, the noise in the higher band will be undersampled by the multiplexing network. Thus the energy of noise can no longer be efficiently filtered out because of the aliasing effects. This will degrade combining gain performance significantly.

B. Internal Loss Components and Noise Figure

The above combining gain analysis is based on an ideal noiseless receiver assumption. However, due to the design goals of the SMILE receiver, an LNA is not the first component in the signal's path after the antenna element; thus noise figure is of concern and in practice this affects the SNR of the system. Each channel has approximately 1.3 dB of insertion loss before the LNA, including the PIN diode and metal loss. This value contributes directly to the noise figure of the system and therefore puts an added strain on the system LNA. With current process technology, it is fairly common to see LNAs with noise figures below 0.5 dB with more than 20 dB gain. Since each channel receives $1/N$ of the signal power compared to that of conventional smart antennas, the LNA gain requirement is increased by $10\log_{10} N$ to retain comparable signal amplitude at the output of the mixer.

C. Experimental Validation

To verify the operation of the complete system, it was tested in an anechoic chamber. A single tone test was performed to evaluate the SMILE system's ability to correctly retain array element phasing through sampling and downconversion. The LO was set to provide a 750-KHz IF with an RF of 5.8 GHz. This test is not used to verify the maximum C/I; hence, its narrow-band nature is not of concern. As long as the sampling rate is fast enough to sample the thermal noise passed by the antenna, problems from the aliasing of noise will not occur. This is not to be confused with maximizing C/I by matching signal and antenna bandwidth.

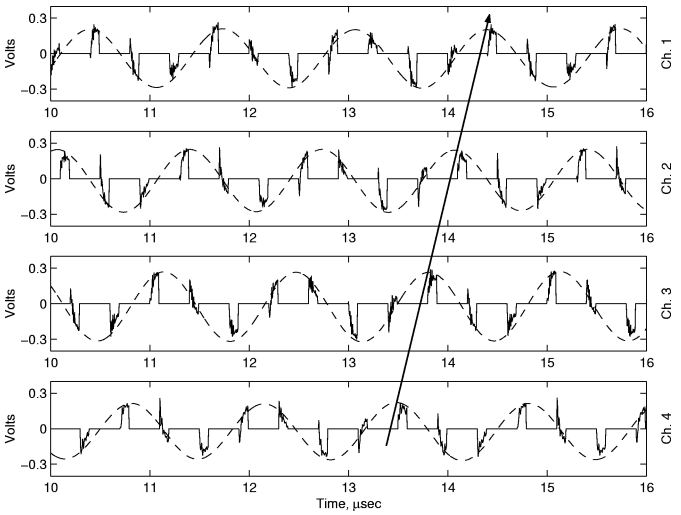

Fig. 3. Measured samples with restored signal envelope.

The array was rotated in 5° steps over ±45° and all four channels of data were recorded. To illustrate the operation, each of the four channels' signals is plotted in Fig. 3 for the array rotated to −30°. Each plot shows the actual samples of the modulated carrier's envelope after demultiplexing but prior to filtering. The dashed sinusoid in each frame is the recovered data after low-pass filtering. A line is drawn along a constant phase front to indicate how the relative phasing between elements varies with array pointing. The noise on the edges of each sample is a result of the PIN diode switch's slow switching speed, not the undersampling of noise. A digital data link test has also been performed demonstrating successful reception and demodulation of a BPSK modulated carrier [1].

III. Antenna Array Feed Network

A four-element patch antenna array is used in this paper. In the schematic of the array shown in Fig. 4, the PIN diodes are located a distance l from the inset feed of each element. The patch array spacing is half a free-space wavelength at the resonance frequency of 5.8 GHz. The patch antennas are on a 62-mil Duroid substrate with dielectric constant $\epsilon_r = 2.33$. Thicker substrate is chosen to increase antenna bandwidth. A comparison of return loss bandwidth for 31- and 62-mil substrates is shown in Fig. 5. A larger bandwidth is desired in order to allow higher data rates to be received. However, the thicker dielectric substrate represents a tradeoff between antenna bandwidth and surface waves, which cause mutual coupling.

The new SMILE technique used in this design necessitates a new type of array feed network. Since array phasing is important, a corporate feed network is integrated with the antenna array. However, as each element is switched ON and OFF, the loading of the antenna to the feed network changes from 50 Ω to an open circuit. A schematic of the feed network used is shown in Fig. 4. In the figure, the switch reference plane is the location

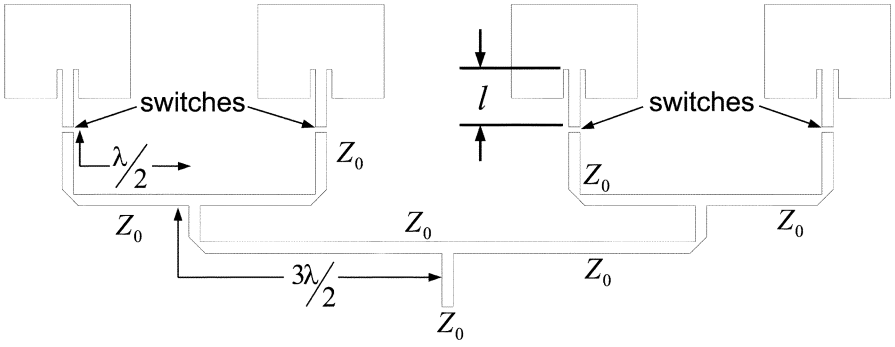

Fig. 4. Schematic of the always matched feed network.

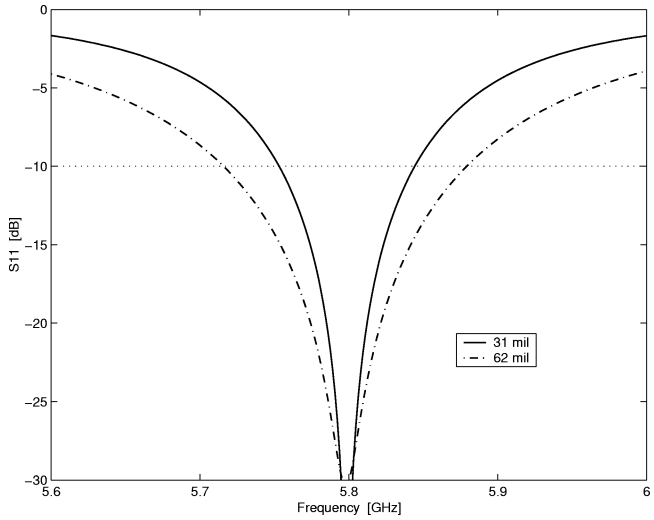

Fig. 5. Patch antenna return loss for different dielectric thickness.

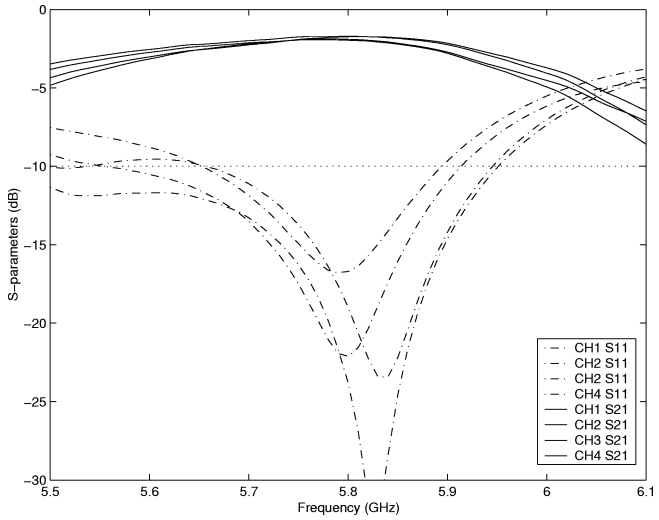

Fig. 6. Measured S-parameters of the always matched feed network.

at which the loading change occurs. The T-like junctions shown are not traditional T-junctions. In this case, all three transmission lines have a characteristic impedance of 50 Ω. The network is designed to always be matched to 50 Ω at its input when exactly one antenna element is active. In order to achieve this goal, the length of the feed lines is tuned in order to bring the open circuit impedance presented by the off-state switch to the edge of the transmission-line junction. Thus the open circuit does not load the feed network. In previous work, the primary goal in the design of the feed network was to maintain the input impedance match. No regard was given to the change in loading to the antenna element that occurs during dynamic switching.

To test the performance of the feed network, a connectorized circuit is assembled with PIN diode switches. Each channel is connected to an Agilent 8510C network analyzer. Measured S-parameters of each channel are shown in Fig. 6. Each individual channel has a bandwidth of more than 200 MHz for a voltage standing-wave ratio less than 2:1. The delay of the feed network poses a return loss bandwidth limitation to the system. Thus, for the feed network presented here, a potential symbol rate of approximately 100 Mbps is allowed. Insertion loss of each channel is approximately 1.7 dB, including 0.4 dB from two SMA connectors and 0.6 dB from the PIN diode. The insertion phase of each channel was verified to be equal. The PIN diodes used in this design are Agilent Technologies beam-lead diodes, HPND-4005, and have an off-state (zero dc bias) isolation of 15 dB. Simulations in Agilent ADS indicate that a static phase error results from adjacent channel leakage at 15 dB below the on-state channel. This error varies with the array's deviation from boresite and active element, with several minima and maxima between 0° and 90°. This error may be compensated for in DSP since it is static in nature. Additional isolation is obtainable with reverse bias at the expense of complicating the switch driver circuit.

IV. Mutual Coupling

The switching of the PIN diode multiplexer causes an impedance loading change to each antenna element. In this section, we will show that the location of the switch along the element feed line has an effect upon mutual coupling. To investigate this phenomena, a brief analysis using the Z-approach is first used. Next the FDTD algorithm is used to examine surface current distributions on a four-element C-band patch antenna array. Once mutual coupling is minimized, radiation patterns are then computed in the next section. In-house FDTD code is used for the surface current investigation because of direct access to solutions of the surface currents.

A. Element Loading Resulting From Array Feed Network

In normal antenna arrays, each antenna element is matched to the system impedance, typically 50 Ω. Thus, each antenna element always has the same loading from the array feed network, and feed network loading does not change as the array operates. However, in the SMILE system, the unique type of feed network creates a wide variation of loading impedance as seen by the antenna element. In the array environment, this change in feed network loading will affect the boundary conditions, which determine the surface currents upon each patch element.

To gain insight into the behavior of the current on each patch, an approximate analysis can be carried out using the coupling matrix approach [5]. The coupling matrix approach models the N-element antenna array as an N-port general microwave network using impedance parameters. Thus, the antenna array may be represented as

$$\begin{aligned} V_1 &= Z_{11}I_1 + \cdots + Z_{1i}I_i + \cdots + Z_{1N}I_N + V_{1,oc} \\ &\vdots \quad\quad \vdots \quad\quad\quad \vdots \quad\quad\quad \vdots \quad\quad \vdots \\ V_i &= Z_{i1}I_1 + \cdots + Z_{ii}I_i + \cdots + Z_{iN}I_N + V_{i,oc} \\ &\vdots \quad\quad \vdots \quad\quad\quad \vdots \quad\quad\quad \vdots \quad\quad \vdots \\ V_N &= Z_{N1}I_1 + \cdots + Z_{Ni}I_i + \cdots + Z_{NN}I_N + V_{N,oc} \end{aligned} \tag{2}$$

where Z_{ii} is the characteristic impedance of the ith antenna element. Z_{ij} is the mutual impedance between the ith and jth elements and $V_{i,oc}$ is the received voltage at the ith port when all other elements are open circuited. The approach does not accurately represent the dynamic nature of the impedance changes in SMILE array, because network theory is based upon the assumption that all ports are always terminated in the characteristic impedance. Yet two important points can be gathered from this approach. First, it is clear that by reducing the I_i terms in (2), mutual coupling will be reduced, and if the I_i terms are augmented, mutual coupling will increase. Second, the analysis assumes the surface currents on the antennas are zero when the ports are open circuited. This approaches the truth only for strongly resonant antennas such as dipole antennas [11]. For general antennas, individual numerical study is required to find the way to reduce the surface currents.

B. Reduction of Surface Currents

Based on the above analysis, it is evident that the reduction of induced surface currents on the adjacent antenna elements may result in reduced antenna mutual coupling. Specifically for the patch antenna array under consideration, the following techniques can be implemented for reduction of surface currents. When an element in the array is connected to the array feed network through a forward biased PIN diode, the element sees a 50-Ω load. However, when the element is OFF, the loading impedance is very high and may be modeled as an open circuit. In order to minimize currents on the surface of the OFF patch, the location of the open circuit should be placed correctly to minimize current on the surface of the element. Each patch antenna is matched to 50 Ω with an inset feed point. Through numerical study, it is found that locating the switch approximately $\lambda_g/4$ from the inset feed point minimizes surface currents. This is because the $\lambda_g/4$ transmission line transforms the open circuit to a short-circuit load in the patch antenna's phase center. Once the phase center is grounded by this load, only minimal currents flow on the surface. Furthermore, if the system is designed without regard to this phenomenon, mutual coupling may be worsened by the array feed network. Since each element is traditionally matched to 50 Ω, the currents must drive this fairly low impedance load. If the location of the switch in the feed network is an odd multiple of $\lambda_g/2$, the element will be loaded with a very high impedance and surface currents may increase.

In order to study the surface currents on the array numerically, an in-house FDTD code was implemented. The FDTD code allows easy access to the surface currents for postprocessing and analysis. The code was used to determine appropriate patch dimensions in an isolated environment. Once the 50-Ω feed point was determined, further simulations were performed in the following manner. One element was selected to be matched to 50 Ω while the other three were to be open circuited. The approximate $\lambda_g/4$ point was selected and simulations were iterated to optimize for minimum surface currents upon the patch. This routine was also performed when the open circuit was located at $\lambda_g/2$ to observe the unwanted maximization of surface currents.

The extent of the FDTD grid in the H plane is much greater than that in the E plane. Therefore, the interelement spacing looks unusually close because the figure is square; however, this is simply a display related issue. The substrate considered is a 62-mil thick material with a relative dielectric constant of $\epsilon_r = 2.33$ and $\tan\delta = 0.002$. The relatively large thickness of the substrate allows a significant amount of current to flow on the substrate as surface waves. This is a tradeoff resulting from the need for additional antenna bandwidth, as surface waves increase the mutual coupling. The current plot shown in Fig. 7(a) is for a single isolated patch element. This provides a reference for comparisons. Fig. 7(b) shows a four-element patch antenna array at 5.8 GHz with every element matched to 50 Ω at all times with the second element being excited. For all cases, the array spacing is $\lambda_0/2$ and the FDTD computation domain remains unchanged.

Fig. 7(c) and (d) illustrates the surface currents for two cases, each with the second antenna element being excited. The first case, shown in Fig. 7(c), is the minimized surface currents as a result of optimization of the switch device location. The second case, shown in Fig. 7(d), illustrates a dramatic increase in surface current intensity in the case of an improperly chosen switch device location.

By comparing the isolated element shown in Fig. 7(a) with the three other cases, it may be observed that the isolated case and the case with the best switch device location have nearly identical current distributions. Elements one and three, in Fig. 7(b), have fairly strong currents on their surfaces. These currents reradiate and cause the mutual coupling affects. Moreover, by comparing surface current intensities between the three array cases (matched to 50 Ω, best, and worst switch device location), it is clear that the best switch device location [Fig. 7(c)] shows a significant reduction in surface current intensity as compared to both the matched case [Fig. 7(b)] and more so the case with the worst switch location [Fig. 7(d)].

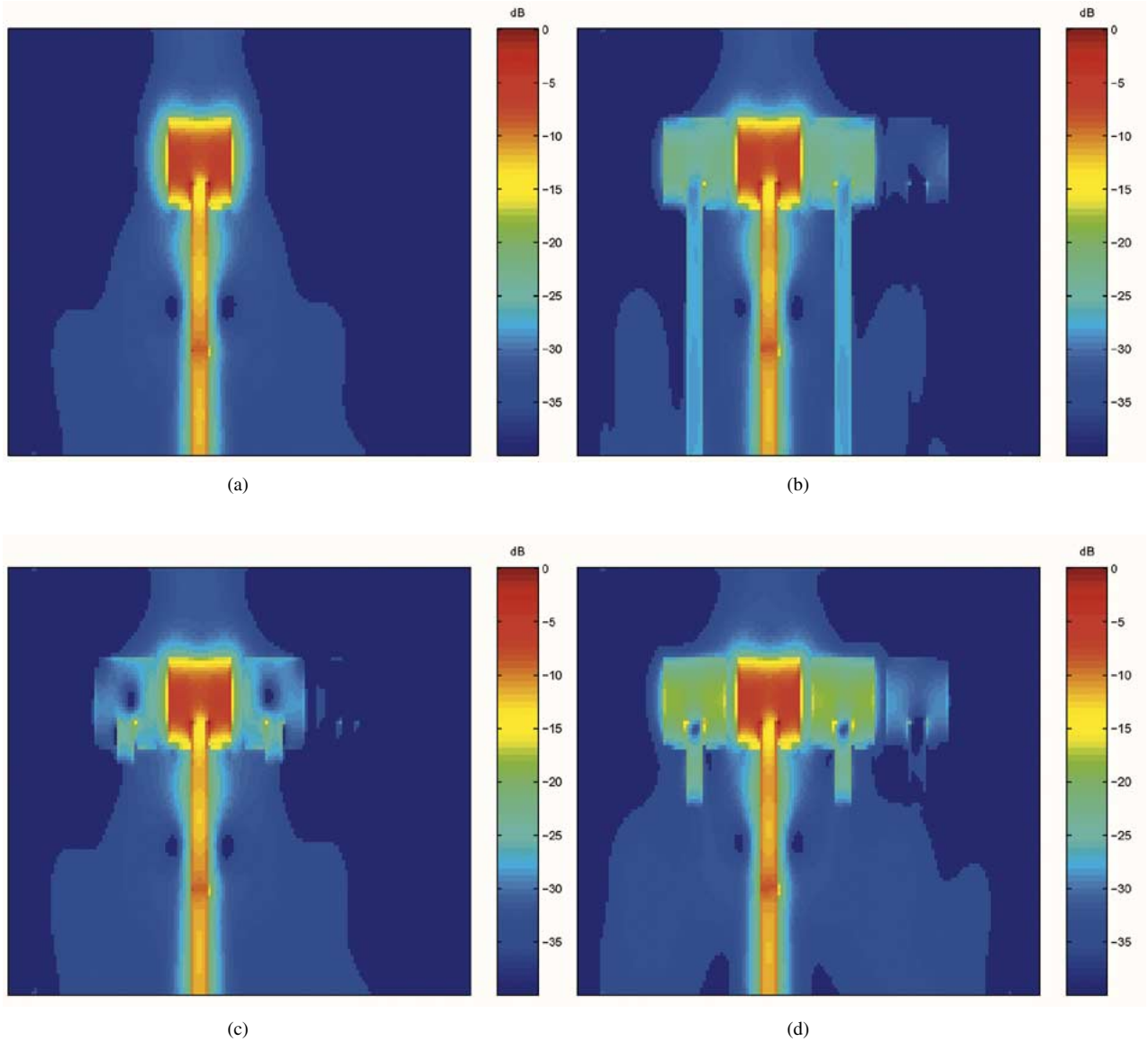

Fig. 7. Currents on the surface of patch antennas for different feed line truncations. (a) Isolated element, (b) four-element array matched to 50 Ω, (c) best switch location, and (d) worst switch location.

It is clear that if the designer of the new SMILE technique smart antenna array system takes into account the switching device's location, a reduction in surface currents is possible. On the contrary, if no regard is given to this design parameter, surface current intensity may actually increase, having a deleterious affect upon the radiation pattern.

C. Other Antenna Element Types

The reduction of mutual coupling in the patch antenna array using the techniques outlined in this transaction may be extended to other types of resonant antennas. The use of the quarter-wavelength transmission line to transform the open-circuited switch to a short circuit at the antenna poses a bandwidth limitation. If a broadband antenna element is used, the short circuit will only be effective near the quarter-wavelength frequency.

V. Radiation Patterns

Once analysis and optimization of the currents on the surface of the patch antenna array were complete, MoM was employed to compute radiation patterns. The choice of momentum MoM over FDTD to compute radiation patterns is because the absorbing boundary condition (ABC) in FDTD truncates the surface currents on the dielectric substrate. This truncation of currents, however small they may be, has an affect on the low level and fine detail in the sidelobes and nulls of the radiation patterns. The infinite ground plane in the MoM solution does not introduce these numerical artifacts.

A. Element Patterns

Prior to examining the radiation patterns of the array environment, it is informative to examine several element pattern cases.

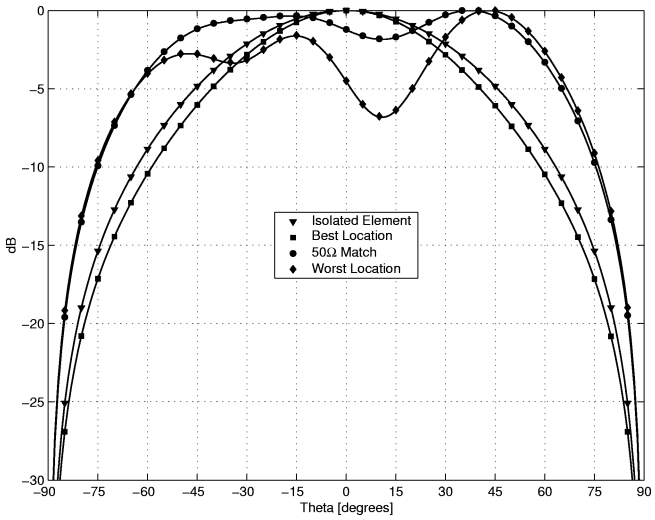

Fig. 8. Active element patterns compared with an isolated element pattern.

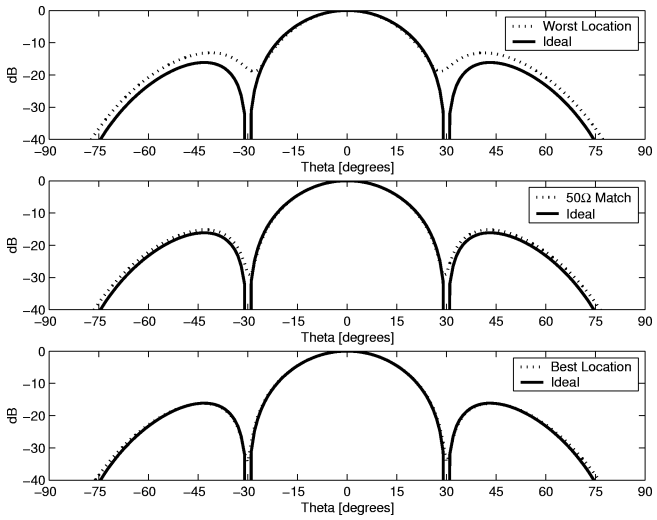

(a)

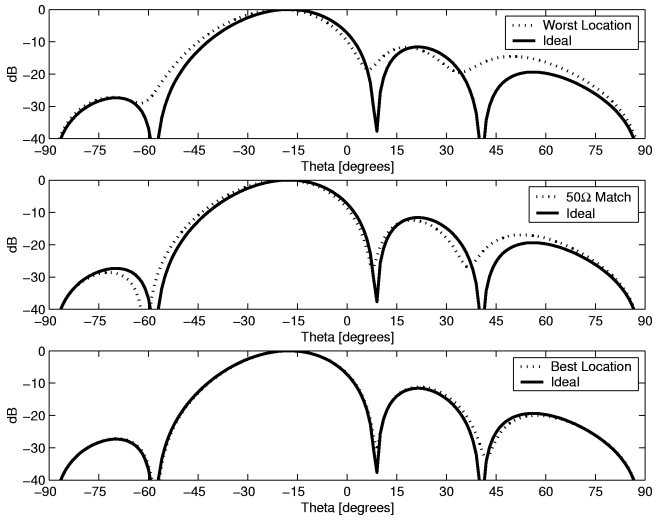

(b)

Fig. 9. Patch antenna array far-field radiation patterns. Array at (a) 0° and (b) −20°.

The optimal radiation pattern is the product of the isolated element pattern and the mathematical array factor for the geometry. Once again, four cases are given to illustrate the work. In each array case the second element is excited. The H plane, copolarized, patterns shown in Fig. 8 give a good idea of exactly how powerful the reduction in mutual coupling may be. The E-plane and cross-polarized patterns remain unchanged from standard cases. The comparison between the isolated element and the best switch device location case shows excellent agreement. Although the beamwidth for the best switch device location case is slightly narrower, its shape and point are nearly ideal. The slight narrowing of the best truncation case is caused by in-phase radiation by the open-circuited elements. The 50-Ω match case shows familiar signs of mutual coupling, namely, the pattern is significantly broader in beamwidth, its peak is tilted toward the right, and the front of the pattern has ripple on the order of 2 dB. Finally, the worst switch device location case shows even more pattern distortion due to mutual coupling. The beam is scanned to approximately $+45^\circ$ and the pattern has a maximum ripple of nearly 7 dB.

The significant improvement in element pattern due to proper switch location is clearly illustrated here.

B. Array Patterns

In order to form the RF array radiation patterns, the dynamic nature of the SMILE smart antenna system must be taken into account. Since at any instant in time only one antenna element is connected to the feed network, it is not possible to form an RF array radiation pattern by coherently exciting all elements in the MoM simulator.

The unit-excitation active element pattern method is employed to calculate the radiation patterns of the three array cases [12]. A third array radiation pattern is calculated by multiplying the pattern of the isolated patch antenna element and a four-element array factor. This pattern is considered the reference pattern, as it is the most desirable case. The unit-excitation method is best suited to cases in which mutual coupling has an effect on the radiation pattern, as in this case. The radiation pattern for each element is computed in the presence of the neighboring parasitic patches using the MoM. Each of the four active-element patterns is then combined with the appropriate spatial phasing to form the array radiation patterns.

The array radiation patterns are shown in Fig. 9(a) for scan angle of 0° (broadside). Each figure shows three frames. Every frame shows the reference radiation pattern calculated from the array factor and isolated element. The top frame compares the reference pattern to a worst location switch device. The sidelobe level at $\pm 45^\circ$, in this case, is 3 dB above the ideal case. The null is almost entirely filled in and its position is shifted. In the middle frame, the 50-Ω matched case has sidelobes that are up by approximately 1 dB; null depth and position are fair. Finally, the lower frame compares the best switch position case with the reference case. In this plot, we see that the sidelobe levels are

identical except at the very far ends of the pattern. The null depth and position are improved over the preceding cases.

The effects of mutual coupling are more pronounced when the radiation patterns are scanned away from broadside. Fig. 9(b) shows three cases scanned to -20° and configured in the same manner as the broadside case, each compared with the ideal radiation pattern. The top frame, comparing worst switch position to the ideal, shows serious radiation pattern distortion. The main beam is broadened and shifted several degrees, nulls are almost completely erased, and sidelobe levels and positions are incorrect. In the middle frame, the 50-Ω case also shows distortion. The main beam is broadened, and some nulls and sidelobes are distorted. The lower frame shows the best results due to minimized surface currents on the adjacent patches. The main beam of the best case is perfectly formed. Sidelobe levels are all within very close tolerances of the ideal pattern, and the null depth and placement are greatly improved.

VI. Conclusion

A new method of reducing mutual coupling in the recently introduced SMILE-type smart antenna receiver has been proposed. The new method utilizes the dynamic switching nature of the SMILE array feed network to reduce mutual coupling. It is shown that proper placement of the switching device in the feed network reduces the magnitude of the surface current on the patch elements not activated by the SMILE system. Through simulations, this reduction in current is shown to improve the active element pattern to nearly the ideal single element pattern. Furthermore, it is shown that the radiation patterns formed by the SMILE smart antenna array using this technique match extremely closely with ideal patterns predicted by theory.

References

[1] J. D. Fredrick, Y. Wang, S. Jeon, and T. Itoh, "A smart antenna receiver array using a single RF channel and digital beamforming," *IEEE Trans. Microwave Theory Tech.*, vol. 50, pp. 3052–3058, Dec. 2002.

[2] K. R. Dandekar, H. Ling, and G. Xu, "Effect of mutual coupling on direction finding in smart antenna applications," *Electron. Lett.*, vol. 36, no. 22, pp. 1889–1891, Oct. 2000.

[3] T. Svantesson, "Direction finding in the presence of mutual coupling,", Chalmers Univ. Tech. Report 307L, 1999.

[4] K. Pasala and E. Friel, "Mutual coupling effects and their reduction in wideband direction of arrival estimation," *IEEE Trans. Aerosp. Electron. Syst.*, vol. 30, pp. 1116–1122, Oct. 1994.

[5] I. J. Gupta and A. A. Ksienski, "Effect of mutual coupling on the performance of adaptive arrays," *IEEE Trans. Antennas Propagat.*, vol. AP-31, pp. 785–791, Sept. 1983.

[6] S. Chen and R. Iwata, "Mutual coupling effects in microstrip patch phased array antenna," in *Proc. IEEE Antennas Propagation Soc. Symp.*, Atlanta, GA, June 1998, pp. 1028–1031.

[7] H. Steyskal and J. S. Herd, "Mutual coupling compensation in small array antennas," *IEEE Trans. Antennas Propagat.*, vol. 38, pp. 1971–1975, Dec. 1990.

[8] M. C. Leifer, "Mutual coupling compensation accuracy," in *Proc. IEEE Antennas Propagation Soc. Symp.*, Boston, MA, July 2001, pp. 804–807.

[9] P. Darwood, P. N. Fletcher, and G. S. Hilton, "Mutual coupling compensation in small planar array antennas," in *Proc. Inst. Elect. Eng. Microwaves, Antennas Propagation*, vol. 145, Feb. 1998, pp. 1–6.

[10] H. M. Aumann, A. J. Fenn, and F. G. Willwerth, "Phased array antenna calibration and pattern prediction using mutual coupling measurements," *IEEE Trans. Antennas Propagat.*, vol. 37, pp. 844–850, July 1989.

[11] T. Su and H. Ling, "On modeling mutual coupling in antenna arrays using the coupling matrix," *Microwave Optical Tech. Lett.*, vol. 28, no. 4, pp. 231–237, Feb. 2001.

[12] D. F. Kelley and W. L. Stutzman, "Array antenna pattern modeling methods that include mutual coupling effects," *IEEE Trans. Antennas Propagat.*, vol. 41, pp. 1625–1632, Dec. 1993.

[13] Y. Qian, W. Dael, N. Kaneda, and T. Itoh, "A uniplanar Quasi-Yagi antenna with wide bandwidth and low mutual coupling characteristics," in *Proc. IEEE Antennas Propagation Soc. Symp.*, Orlando, FL, July 1999, pp. 924–927.

Jonathan D. Fredrick (S'95–M'02) was born in Queens, NY, in 1975. He received the B.S. degree from the State University of New York (SUNY), College at New Paltz, in 1997 and the M.S. and Ph.D. degrees from the University of California, Los Angeles, in 2000 and 2002, respectively, all in electrical engineering.

From 1998 to 2002, he was a Graduate Student Research Assistant in the Electrical Engineering Department, University of California, Los Angeles (UCLA). He is currently with Raytheon Space and Airborne Systems, El Segundo, CA. His research interests at UCLA were on smart antenna receiver arrays and true time delay lines for wireless communications, microwave circuits, integrated circuits, and antennas.

Dr. Fredrick received an IEEE MTT-S Graduate Student Fellowship in 1999 and 2001, won first place in the Best Student Paper Competition at the 29th European Microwave Conference in Munich, Germany in 1999, and won second place in the student paper competition at IMS 2002, Seattle, WA.

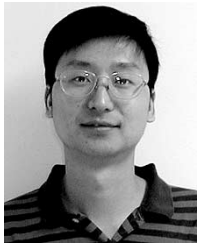

Yuanxun Wang (S'96–M'99) received the B.S. degree from the University of Science and Technology of China (USTC), Hefei, in 1993 and the M.S. and Ph.D. degrees from the University of Texas at Austin, in 1996 and 1999, respectively, all in electrical engineering.

From 1993 to 1995, he was a Graduate Researcher with USTC on numerical methods and millimeter-wave radar-based instruments. From 1995 to 1999, he was with the Department of Electrical and Computer Engineering, University of Texas at Austin, as a Graduate Research Assistant working on radar scattering modeling and synthetic aperture radar imaging. From 1999 to 2002, he was a Research Engineer and Lecturer in the Department of Electrical Engineering, University of California at Los Angeles (UCLA), prior to joining the Faculty. He has been an Assistant Professor in the Electrical Engineering Department since November 2002. His current work is focused on high-performance antenna array and microwave amplifier systems for wireless communication and radar, as well as numerical modeling techniques. His research interests feature the fusion of signal-processing and circuit techniques in microwave system design. He has authored and coauthored over 60 refereed journal and conference papers.

Prof. Wang is a Member of The International Society for Optical Engineers (SPIE), Bellingham, WA.

Tatsuo Itoh (S'69–M'69–SM'74–F'82) received the Ph.D. degree in electrical engineering from the University of Illinois, Urbana-Champaign, in 1969.

From 1966 to 1976, he was with the Electrical Engineering Department, University of Illinois. From 1976 to 1977, he was a Senior Research Engineer in the Radio Physics Laboratory, SRI International, Menlo Park, CA. From 1977 to 1978, he was an Associate Professor at the University of Kentucky, Lexington. In 1978, he joined the Faculty at The University of Texas at Austin, where he became a Professor of electrical engineering in 1981 and Director of the Electrical Engineering Research Laboratory in 1984. During the summer of 1979, he was a Guest Researcher at AEG-Telefunken, Ulm, West Germany. In 1983, he became Hayden Head Centennial Professor of Engineering at The University of Texas. In 1984, he became Associate Chairman for Research and Planning of the Electrical and Computer Engineering Department, The University of Texas. In 1991, he joined the University of California, Los Angeles, as Professor of electrical engineering and holder of the TRW Endowed Chair in Microwave and Millimeter Wave Electronics. He was an Honorary Visiting Professor at Nanjing Institute of Technology, China, and at the Japan Defense Academy. In 1994, he became Adjunct Research Officer for Communications Research Laboratory, Ministry of Post and Telecommunication, Japan. He currently holds a Visiting Professorship at the University of Leeds, U.K., and is an External Examiner of the Graduate Program, City University of Hong Kong. He has 280 journal publications and 585 refereed conference presentations. He has written 30 books/book chapters in the area of microwaves, millimeter-waves, antennas, and numerical electromagnetics. He has supervised 49 Ph.D. students.

Dr. Itoh is a Member of the Institute of Electronics and Communication Engineers of Japan, and Commissions B and D of USNC/URSI. He was elected an Honorary Life Member of the MTT Society in 1994. He has received a number of awards, including the Shida Award from the Japanese Ministry of Post and Telecommunications in 1998, Japan Microwave Prize in 1998, IEEE Third Millennium Medal in 2000, and IEEE MTT Distinguished Educator Award in 2000. In 2001, he received the Nikola Tesla Award from the Serbian Academy of Science and Arts in Yugoslavia. He was Chairman of USNC/URSI Commission D from 1988 to 1990 and Chairman of Commission D of the International URSI for 1993–1996. He is Chair of the Long Range Planning Committee of URSI. He serves on advisory boards and committees of a number of organizations. He was Editor of IEEE TRANSACTIONS ON MICROWAVE THEORY AND TECHNIQUES for 1983–1985 and Editor-in-Chief of IEEE MICROWAVE AND GUIDED WAVE LETTERS from 1991 through 1994. He is on the Administrative Committee of IEEE Microwave Theory and Techniques Society. He was Vice President of the Microwave Theory and Techniques Society in 1989 and President in 1990.